Regulation of yeast ESCRT-III membrane scission activity by the Doa4 ubiquitin hydrolase

Natalie Johnson, Matt West, and Greg Odorizzi*
Molecular, Cellular, and Developmental Biology, University of Colorado, Boulder, CO 80309

ABSTRACT **ESCRT-III executes membrane scission during the budding of intralumenal vesicles (ILVs) at endosomes. The scission mechanism is unknown but appears to be linked to the cycle of assembly and disassembly of ESCRT-III complexes at membranes. Regulating this cycle is therefore expected to be important for determining the timing of ESCRT-III–mediated membrane scission. We show that in *Saccharomyces cerevisiae*, ESCRT-III complexes are stabilized and ILV membrane scission is delayed by Doa4, which is the ubiquitin hydrolase that deubiquitinates transmembrane proteins sorted as cargoes into ILVs. These results suggest a mechanism to delay ILV budding while cargoes undergo deubiquitination. We further show that deubiquitination of ILV cargoes is inhibited via Doa4 binding to Vps20, which is the subunit of ESCRT-III that initiates assembly of the complex. Current models suggest that ESCRT-III complexes surround ubiquitinated cargoes to trap them at the site of ILV budding while the cargoes undergo deubiquitination. Thus our results also propose a mechanism to prevent the onset of ILV cargo deubiquitination at the initiation of ESCRT-III complex assembly.**

Monitoring Editor
Sandra Lemmon
University of Miami

Received: Nov 4, 2016
Revised: Dec 15, 2016
Accepted: Dec 30, 2016

INTRODUCTION

Endosomal sorting complexes required for transport (ESCRTs) execute membrane remodeling and scission (reviewed in Hurley, 2015). ESCRTs were originally characterized on the basis of their activities at endosomes in *Saccharomyces cerevisiae*, where they function in the formation of intralumenal vesicles (ILVs) that are degraded in the hydrolytic interior of vacuolar lysosomes upon endolysosomal fusion (Katzmann *et al.*, 2001; Babst *et al.*, 2002a,b). The role ESCRTs have in the ILV budding pathway is conserved throughout eukaryotes (Hanson and Cashikar, 2012). Studies in vitro support a model in which ESCRT-I and -II initiate ILV budding by inducing membrane invagination, and ESCRT-III completes the process by constricting the membrane and catalyzing the scission reaction that detaches nascent ILV buds (Wollert *et al.*, 2009; Wollert and Hurley, 2010). Ubiquitinated transmembrane proteins targeted for lysosomal degradation are sorted into ILVs by ESCRT-0, -I, and -II, each of which has one or more ubiquitin-binding domains (Katzmann *et al.*, 2001; Bilodeau *et al.*, 2002; Alam *et al.*, 2004).

Among ESCRTs, the most deeply conserved are subunits of the ESCRT-III complex and its regulatory ATPase, Vps4. Orthologues of ESCRT-III and Vps4 are in Archaea, where they function in cell division (Samson *et al.*, 2008). In eukaryotes, the ESCRT-III/Vps4 machinery similarly functions during cytokinesis to constrict and sever membrane necks connecting daughter cells (Carlton and Martin-Serrano, 2007). This activity is exploited by HIV-1 and other retroviruses, which recruit ESCRT-III and Vps4 to bud from the plasma membrane of infected cells (Garrus *et al.*, 2001). Membrane scission by ESCRT-III might also be involved in other processes in which this machinery has more recently been found to be required, including plasma membrane wound repair (Jimenez *et al.*, 2014), nuclear pore complex quality control (Webster *et al.*, 2014), and postmitotic nuclear envelope reformation (Olmos *et al.*, 2015; Vietri *et al.*, 2015).

The biophysical mechanism of membrane scission executed by ESCRT-III is unknown (Hurley, 2015), but insights have come from understanding the assembly and disassembly of ESCRT-III complexes. ESCRT-III subunits are homologous to one another, and each subunit cycles between two conformational states in which the closed/inactive form is a soluble monomer in the cytosol and the open/active form oligomerizes with other subunits of the complex at the cytosolic surface of the membrane (Babst *et al.*, 2002b; Shim *et al.*, 2007). Genetic and biochemical studies in yeast indicate that the four core subunits of ESCRT-III undergo ordered assembly: Vps20 nucleates homopolymerization of Snf7, and growth of the

This article was published online ahead of print in MBoC in Press (http://www.molbiolcell.org/cgi/doi/10.1091/mbc.E16-11-0761) on January 5, 2017.

*Address correspondence to: Greg Odorizzi (odorizzi@colorado.edu).

Abbreviations used: BiFC, bimolecular fluorescence complementation; BMV, brome mosaic virus; ESCRT, endosomal sorting complex required for transport; ILV, intralumenal vesicle; MIM, microtubule-interacting motif; MIT, microtubule-interacting and -trafficking; TBSV, tomato bushy stunt virus.

Snf7 polymer is capped upon its association with the Vps2 and Vps24 subunits of the complex (Teis *et al.*, 2008; Saksena *et al.*, 2009). ESCRT-III complex assembly proceeds in a spiral pattern on the membrane that surrounds the site at which scission will occur (Hanson *et al.*, 2008), and studies in vitro indicate that the capping step of assembly converts ESCRT-III from flat spirals into a spring-like conformation, which might facilitate membrane constriction and/or scission (Henne *et al.*, 2012; Chiaruttini *et al.*, 2015).

ESCRT-III assembly at endosomes is required to trap the ubiquitinated transmembrane protein cargoes sorted by ESCRT-0, -I, and II, suggesting that ESCRT-III complexes encircle cargoes to prevent their diffusion away from the site of ILV budding while the cargoes undergo deubiquitination (Teis *et al.*, 2010). Doa4 is the ubiquitin hydrolase that deubiquitinates ILV cargoes in yeast (Dupre and Haguenauer-Tsapis, 2001; Katzmann *et al.*, 2001; Losko *et al.*, 2001), and its function prevents the ILV budding pathway from depleting the cellular supply of free, nonconjugated ubiquitin (Swaminathan *et al.*, 1999). The function of Doa4 at the site of ESCRT-III assembly is regulated by an ESCRT-III–associated protein, Bro1, which facilitates the recruitment of Doa4 to endosomes (Luhtala and Odorizzi, 2004). Bro1 also directly binds the Doa4 catalytic domain to stimulate its ubiquitin hydrolase activity (Richter *et al.*, 2007).

ESCRT-III complex disassembly is catalyzed by Vps4 (Babst *et al.*, 1998), which is a member of the AAA+ family of ATPases that unfold proteins and/or disassemble protein complexes. The amino terminus of Vps4 consists of a microtubule-interacting and -trafficking (MIT) domain that binds two distinct MIT-interacting motifs (MIMs; MIM1 and MIM2) located at or near the carboxyl termini of ESCRT-III subunits (Obita *et al.*, 2007; Stuchell-Brereton *et al.*, 2007; Kieffer *et al.*, 2008). In the case of Snf7, MIM2 binds the Vps4 MIT domain, but MIM1 of Snf7 binds the "Bro1 domain," which is located at the amino terminus of Bro1 and is structurally dissimilar to the MIT domain of Vps4 (Kim *et al.*, 2005). Binding of the Bro1 domain to Snf7 mediates Bro1 recruitment to ESCRT-III and is therefore essential for Bro1 to promote ILV cargo deubiquitination by Doa4 (Wemmer *et al.*, 2011). However, Bro1 domain binding also protects Snf7 from disassembly by Vps4, and overexpression of Bro1 or the Bro1 domain in yeast delays ILV membrane scission (Wemmer *et al.*, 2011). Thus another function of Bro1 is the control of ESCRT-III membrane scission activity through its regulation of ESCRT-III complex stability, but the way in which Bro1 achieves this regulation is unknown.

We previously reported that MIM1 in the Vps20 subunit of ESCRT-III binds an MIT-like domain at the amino terminus of Doa4 and that this interaction inhibits a noncatalytic function of Doa4 that promotes the ILV budding pathway through an unknown mechanism (Richter *et al.*, 2013). Here we show that Doa4 functions noncatalytically to regulate ILV membrane scission by stabilizing ESCRT-III complexes. We further show that both the catalytic and noncatalytic functions of Doa4 are inhibited through its binding to Vps20, which is the subunit of ESCRT-III that initiates complex assembly. Overexpression of the *BRO1* gene inhibits Doa4 binding to Vps20, revealing another mechanism by which Bro1 promotes Doa4 function. Collectively our results suggest a model for bidirectional regulation between ESCRT-III and the deubiquitination machinery of the ILV budding pathway.

RESULTS

Doa4 cooperates with Bro1 to stabilize ESCRT-III complexes

The stability of ESCRT-III complexes is defined by their steady-state abundance, which is determined by the rate of complex assembly offset by the rate of complex disassembly (Figure 1A).

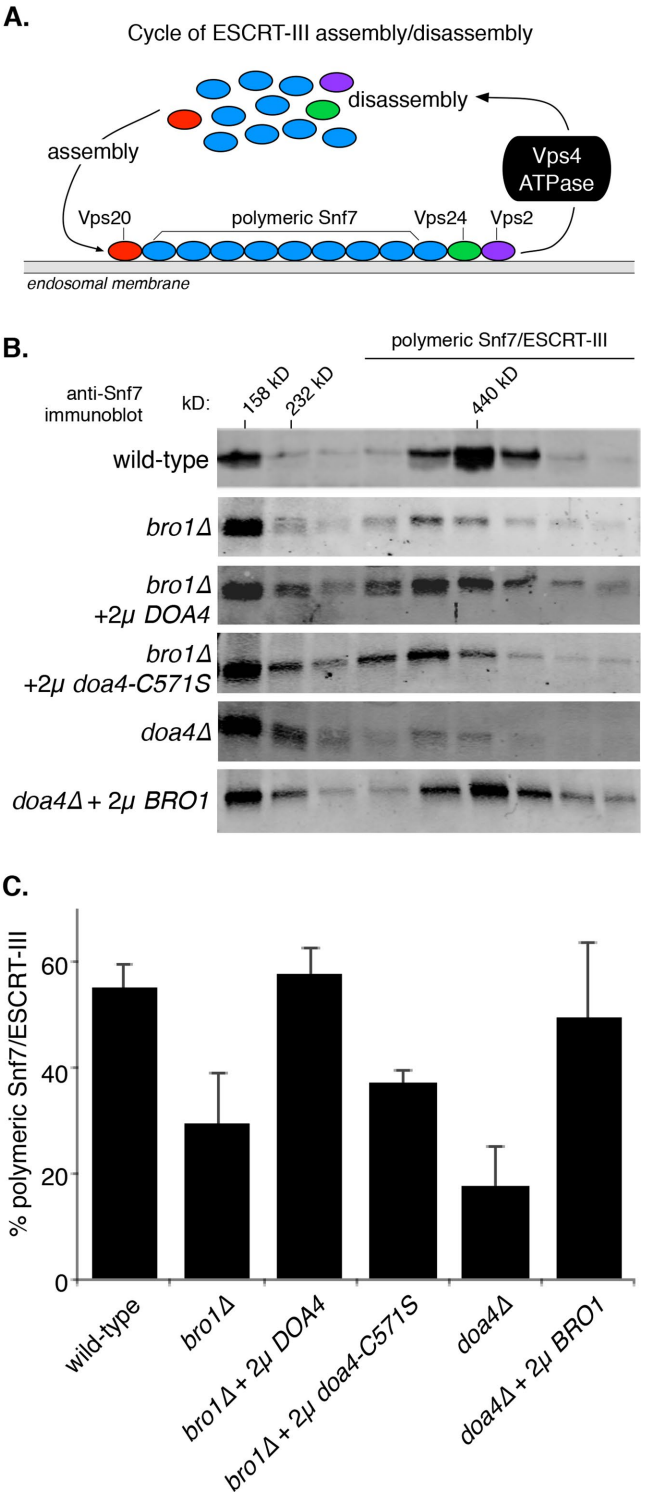

FIGURE 1: Doa4 cooperates with Bro1 to stabilize ESCRT-III complexes. (A) Cycle of ESCRT-III assembly and disassembly. (B) Western blot analysis of the distribution of Snf7 in fractions resolved by rate-zonal density gradient centrifugation. Indicated at the top are migrations of molecular weight standards: aldolase (156 kDa), catalase (232 kDa), and ferritin (440 kDa). (C) Quantitations from triplicate experiments of the percentage of Snf7 in all gradient fractions represented by polymeric Snf7/ESCRT-III in fractions 4–9; this size range was previously established to correspond to assembled ESCRT-III complexes (Teis *et al.*, 2008). Error bars represent SDs.

ESCRT-III complex stability can therefore be assayed in yeast based on sedimentation of the most abundant subunit of the complex, Snf7, after rate-zonal centrifugation of detergent-solubilized membranes (Teis *et al.*, 2008). Using this approach, we found that deletion of the *BRO1* gene caused a 50% decrease in the amount of polymeric Snf7 (Figure 1, B and C) without noticeably affecting the overall cellular abundance of Snf7 protein (Supplemental Figure S1) or the amount of membrane-associated Snf7 (Supplemental Figure S2). This observation agrees with our previous finding that Bro1 functions to stabilize ESCRT-III complexes by inhibiting their disassembly (Wemmer *et al.*, 2011).

In addition to its role in promoting ESCRT-III complex stability, Bro1 stimulates the ubiquitin hydrolase activity of Doa4. We originally identified a role for Bro1 in regulating Doa4 by finding that *DOA4* overexpression rescued ILV cargo sorting in cells lacking Bro1 function (Luhtala and Odorizzi, 2004). Figure 1, B and C, shows that overexpression of *DOA4* also fully rescued ESCRT-III complex abundance in *bro1*Δ cells and that partial rescue was provided by overexpression of the catalytically inactive *doa4-C571S* allele. These observations suggested that Doa4 functions to cooperate with Bro1 in promoting ESCRT-III complex stability. This hypothesis was supported by our observation that deletion of the *DOA4* gene (*doa4*Δ) caused a strong reduction in ESCRT-III complexes, much like what we saw in *bro1*Δ cells (Figure 1, B and C, and Supplemental Figures S1 and S2). Furthermore, the abundance of ESCRT-III complexes in *doa4*Δ cells was restored to wild-type levels when *BRO1* was overexpressed, similar to the replenishment of ESCRT-III abundance in *bro1*Δ cells overexpressing *DOA4* (Figure 1, B and C). Excess levels of either Doa4 or Bro1 can therefore maintain normal ESCRT-III complex stability when the other protein is absent.

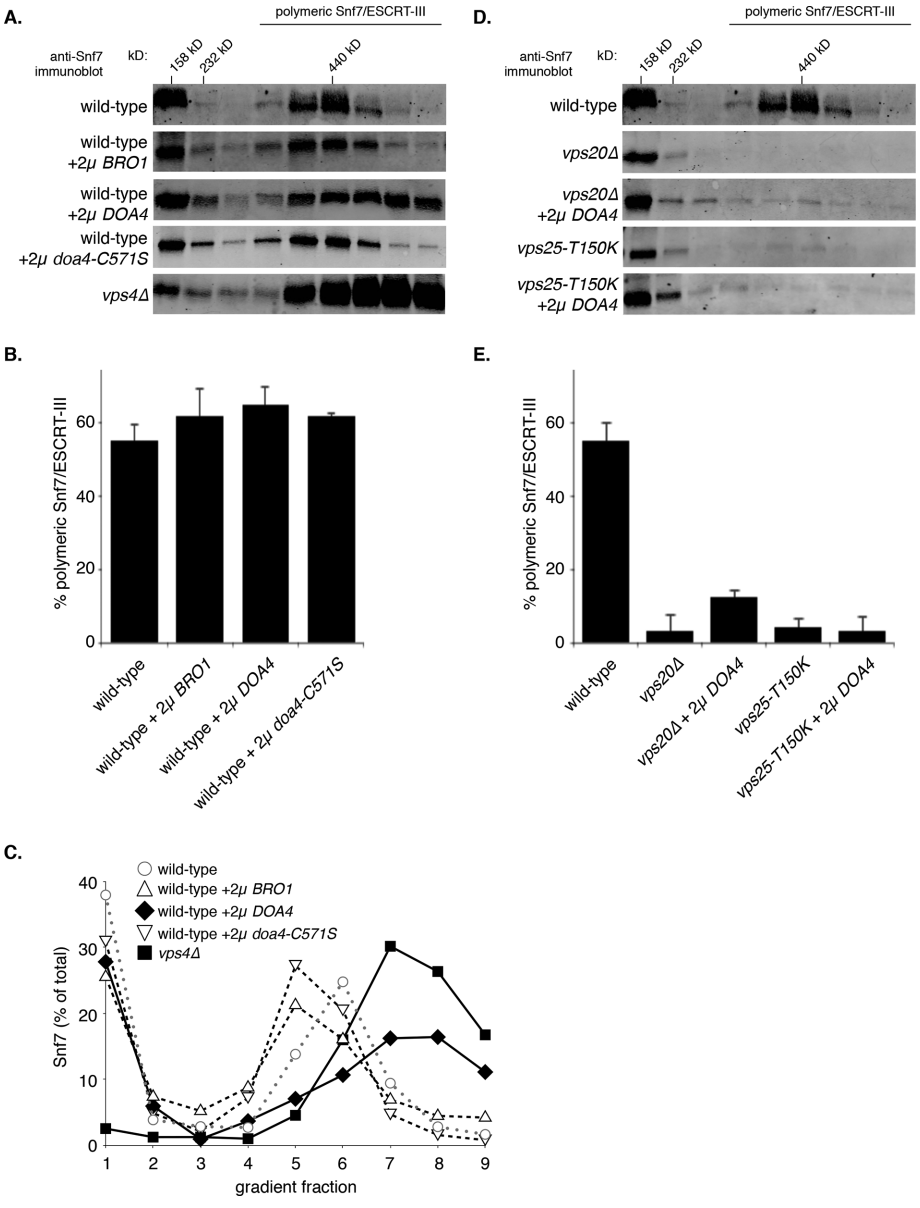

FIGURE 2: *DOA4* overexpression causes accumulation of high–molecular weight ESCRT-III complexes. Western blot analysis (A, D) and quantitation (B, E) of polymeric Snf7/ESCRT-III as described in Figure 1. Wild-type results in A and D are identical. (C) Line-graph representation of the mean percentage of membrane-associated Snf7 in each gradient fraction from the indicated strains examined in triplicate experiments; SD values are omitted for clarity.

DOA4 overexpression causes accumulation of high–molecular weight ESCRT-III complexes

We previously saw a moderate increase in ESCRT-III complex stability in wild-type cells when *BRO1* was overexpressed, consistent with Bro1 functioning to inhibit disassembly of the complex (Wemmer *et al.*, 2011; Figure 2, A and B). *DOA4* overexpression in wild-type cells had a similar effect (Figure 2, A and B), which was not surprising, given that high-copy *DOA4* rescued ESCRT-III complex stability in cells lacking Bro1 (Figure 1). The abundance of ESCRT-III complexes also increased when *doa4-C571S* was overexpressed in wild-type cells (Figure 2, A and B), echoing the result in Figure 1, which indicated that the ubiquitin hydrolase activity of Doa4 is not essential for it to promote ESCRT-III complex stability.

A notable difference upon overexpression of wild-type *DOA4* was the accumulation of higher–molecular weight ESCRT-III complexes, the size range of which was similar to that seen in cells lacking the Vps4 ATPase that disassembles ESCRT-III (*vps4*Δ; Figure 2, A and C). This observation suggested that *DOA4* overexpression boosts the abundance of ESCRT-III complexes by inhibiting their disassembly, although an alternative possibility is that Doa4 stimulates complex assembly. However, *DOA4* overexpression did not rescue ESCRT-III complex abundance in either *vps20*Δ or *vps25-T150K* cells (Figure 2, E and F), the latter of which express a mutant version of the ESCRT-II complex that is unable to bind and activate Vps20 (Im *et al.*, 2009; Teis *et al.*, 2010). Therefore Doa4 cannot augment the canonical pathway for ESCRT-III complex assembly (Saksena *et al.*, 2009; Teis *et al.*, 2010), suggesting that Doa4 stabilizes ESCRT-III complexes by inhibiting their disassembly rather than by stimulating complex assembly.

DOA4 overexpression delays ILV membrane scission

We previously showed by electron tomography and three-dimensional (3D) modeling of yeast endosomes that *BRO1* overexpression in wild-type cells delays ILV membrane scission (Wemmer *et al.*, 2011). This corroborated other studies suggesting that the membrane scission activity of ESCRT-III is linked to Vps4-mediated disassembly of the complex (Sachse *et al.*, 2004; Hanson *et al.*, 2008). On the basis of our finding that Doa4 could function similar to Bro1 toward stabilizing ESCRT-III complexes, we examined endosomes by tomography in wild-type yeast with or without *DOA4* overexpression.

As in our previous study (Wemmer *et al.*, 2011), we measured an average of 1.2 ILV budding profiles per endosome in wild-type cells, and this frequency was nearly doubled by *BRO1* overexpression (Figure 3, A and D). *DOA4* overexpression had a much stronger effect. Endosomes had an average of 5.0 ILV budding profiles in wild-type cells overexpressing *DOA4*, which is >4.5-fold the amount normally seen and >2.5-fold the amount observed upon *BRO1* overexpression (Figure 3, B and D). *DOA4* overexpression also caused a sharper reduction in ILV budding than did *BRO1* overexpression, indicating that Doa4 more strongly inhibited ILV membrane scission. Measurements of lumenal versus limiting endosomal membrane surface areas showed that ILVs account for ~55% of the total membrane at each endosome in wild-type yeast; *DOA4* overexpression caused a 40% reduction in this amount, whereas *BRO1* overexpression reduced the ILV membrane content by only 20% (Figure 3E). Overexpression of the mutant *doa4-C571S* allele also increased the frequency of ILV budding profiles, although only to the extent seen upon *BRO1* overexpression (Figure 3, C and D). Although this observation is consistent with its ubiquitin hydrolase function being dispensable for ESCRT-III regulation (Figures 1 and 2), a potential role for Doa4 catalytic activity in ESCRT-III regulation cannot be ruled out because *doa4-C571S* overexpression did not decrease the ILV content of endosomes (Figure 3E).

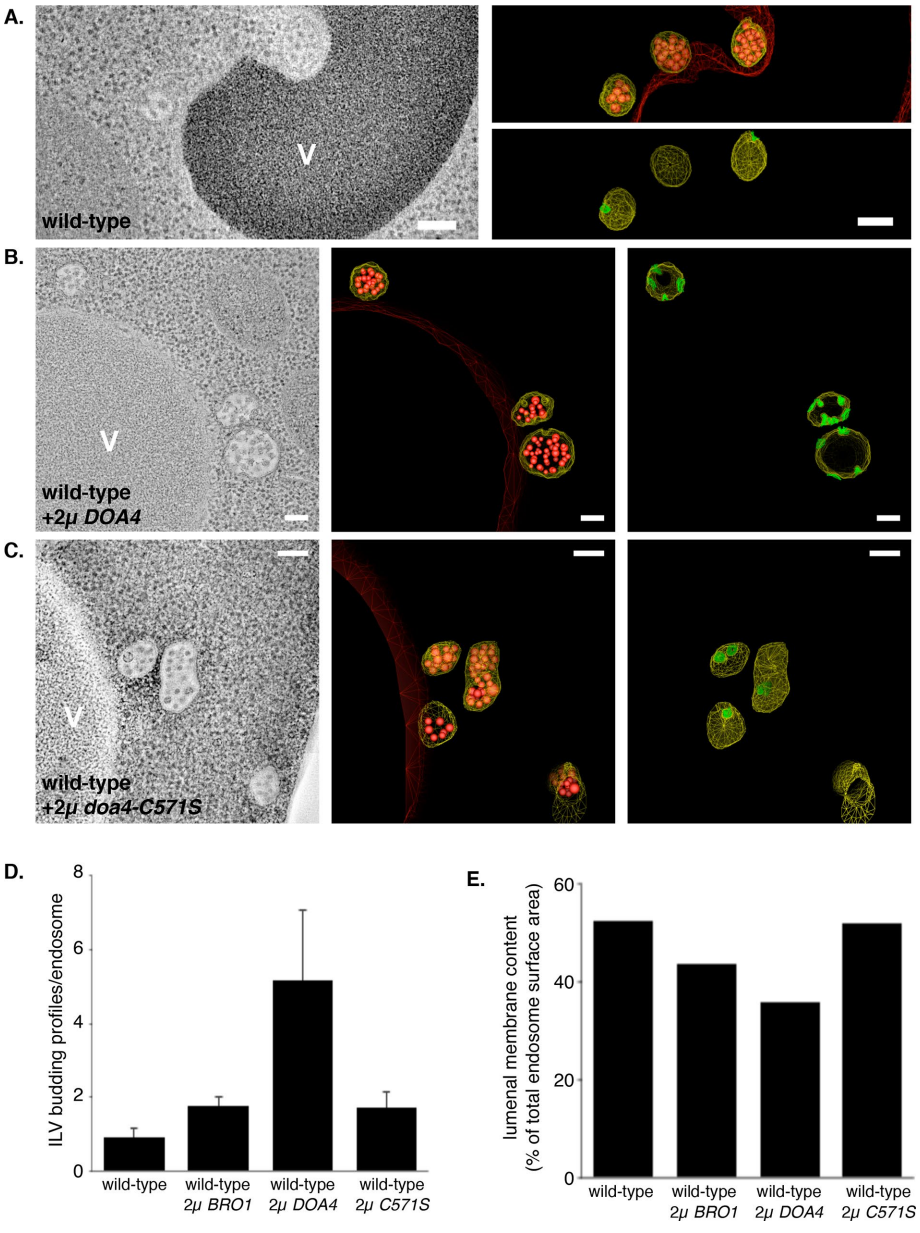

FIGURE 3: *DOA4* overexpression delays ILV membrane scission. (A–C) Two-dimensional cross-sectional tomographic slices and 3D models from 250-nm-thick section electron tomographs. In each model, spherical endosomal limiting membranes are traced in yellow, freely detached ILVs are traced in red, and ILV budding profiles are traced in green. In some cases, the continuity of ILV budding profiles with the limiting endosomal membrane is out of plane in the tomographic slice but evident in the 3D reconstruction. Bars, 100 nm. ILV budding profiles were identified by negative curvature and a net surface area greater than one-half of the mean ILV surface (>750 nm^2). (D) Quantitation of ILV budding profiles per endosome from tomographs and models of wild-type cells alone (WT; $N = 12$) vs. wild-type cells transformed with a high–copy number plasmid (*2μ*) encoding *BRO1* ($N = 17$), *DOA4* ($N = 7$), or *doa4-C571S* ($N = 14$); error bars represent SDs. (E) Quantitation of the lumenal vs. limiting membrane surface areas in modeled endosomes. Quantitative data for *2μ BRO1* transformants are derived from experiments in Wemmer *et al.* (2011).

The Vps20 subunit of ESCRT-III inhibits complex stabilization by Doa4

The foregoing observations indicated that Doa4 regulates ESCRT-III complex stability and ILV membrane scission, and it appears to do so in a manner that does not depend upon its ubiquitin hydrolase activity. We had previously reported a noncatalytic role for Doa4 that rescues ILV budding when Bro1 is absent and showed that this function of Doa4 is inhibited through Doa4 binding to the MIM1 site in Vps20; thus the ILV-budding pathway was rescued in *bro1Δ* cells upon point mutation of the Vps20 MIM1 sequence (Richter *et al.*, 2013). Figure 4, A and B, shows that the *vps20-ΔMIM1* mutation also rescued ESCRT-III complex stability in *bro1Δ* cells, whereas the *vps20-ΔMIM1* mutation on its own had no apparent effect toward ESCRT-III. Of importance, the rescue of ESCRT-III complex stability seen in *bro1Δ vps20-ΔMIM1* cells required Doa4 but not its ubiquitin

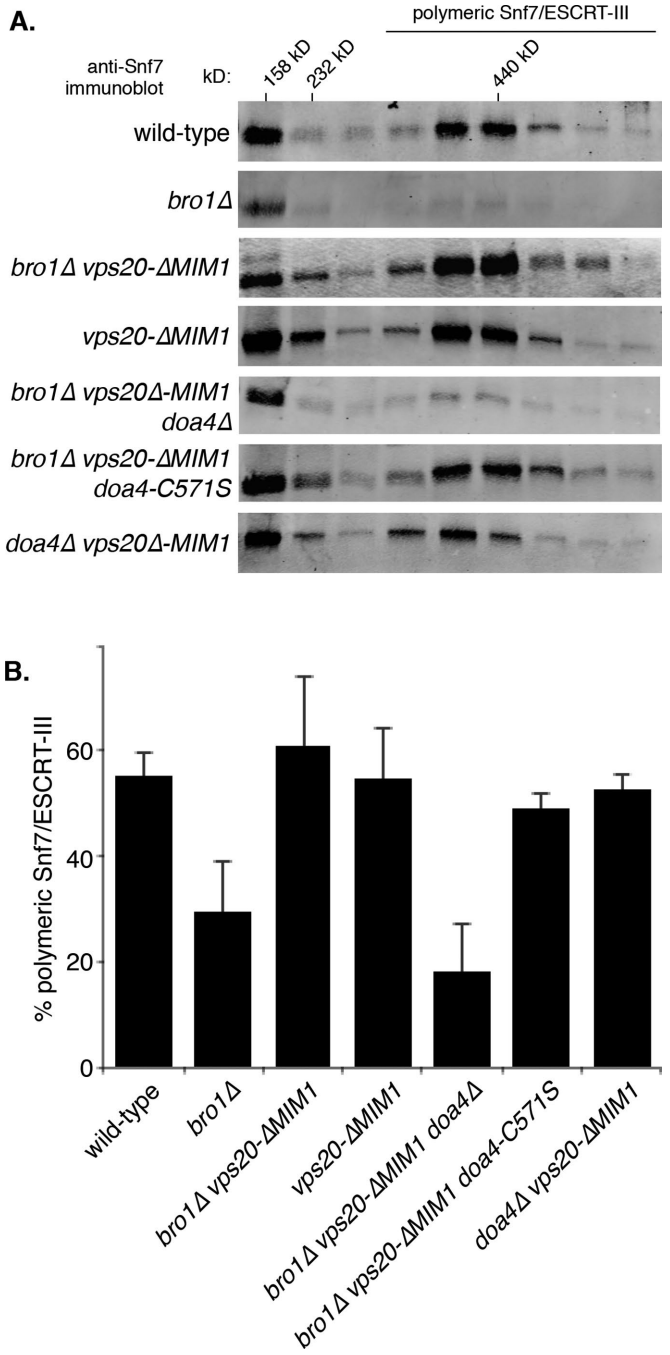

FIGURE 4: The Vps20 subunit of ESCRT-III inhibits complex stabilization by Doa4. Western blot analysis (A) and quantitation from triplicate experiments (B) of polymeric Snf7/ESCRT-III as described in Figure 1.

hydrolase activity because rescue still occurred upon replacing wild-type *DOA4* with the *doa4-C571S* allele, whereas deletion of the *DOA4* gene prevented rescue (Figure 4, A and B). Therefore the noncatalytic function Doa4 has toward stabilizing ESCRT-III complexes is inhibited through its interaction with the MIM1 sequence in the Vps20 subunit of ESCRT-III. Moreover, expression of *BRO1* in *doa4Δ vps20-ΔMIM1* cells sustained wild-type levels of polymeric Snf7 (Figure 4, A and B), which was not surprising, given the data in Figure 1 showing that either Bro1 and Doa4 can maintain Snf7 complex stability.

Bro1 relieves Vps20 inhibitory binding to Doa4

Inhibitory binding exerted by Vps20 toward Doa4 is presumably dynamic in yeast to ensure that Doa4 regulation of ESCRT-III is spatiotemporally controlled. Transient binding between Vps20 and Doa4 would explain why their coimmunoprecipitation from yeast could not be detected without disabling the Vps4 ATPase that disassembles ESCRT-III (Richter *et al.*, 2013). Further evidence that Vps20 transiently binds Doa4 in vivo was provided through bimolecular fluorescence complementation (BiFC) studies in which we expressed in yeast either the amino- or carboxyl-terminal fragments of the Venus fluorescent protein (VN and VC, respectively) fused to the carboxyl terminus of Doa4 versus Vps20. Binding between Doa4 and Vps20 would bring the VN and VC fragments within close proximity, allowing the Venus reporter to assemble into its native 3D structure and emit a fluorescence signal (Kerppola, 2006). Of importance, assembly of the Venus protein in this experimental system is irreversible, which means that the normal association/dissociation cycle of proteins interacting dynamically with one another is disrupted; therefore the interaction between Doa4-VN and Vps20-VC would be stabilized through assembly of the Venus reporter protein.

Previous studies individually examining the localizations of Vps20 and Doa4 showed that each protein associates with endosomal puncta (Amerik *et al.*, 2000; Babst *et al.*, 2002b; Luhtala and Odorizzi, 2004). Thus we expected cells coexpressing Doa4-VN and Vps20-VC to exhibit BiFC fluorescence at endosomes. Instead, fluorescence was seen within the vacuole lumen, which depended upon Doa4 binding to the Vps20 MIM1 sequence because fluorescence was absent from cells coexpressing Doa4-VN and Vps20-ΔMIM1-VC (Figure 5A).

BiFC fluorescence in the vacuole lumen suggested that the irreversibly assembled Doa4-VN/Vps20-VC complexes were aberrantly sorted as "cargoes" into ILVs that were subsequently delivered into the vacuole lumen upon endolysosomal fusion. A similar case of mistaken identity had been reported previously for a mutant ESCRT-I complex lacking one of its subunits (Curtiss *et al.*, 2007). The irreversible assembly of Doa4-VN/Vps20-VC complexes did not block the ILV-budding pathway because BiFC fluorescence within vacuoles expressing Doa4-VN and Vps20-VC colocalized with Cps1, a canonical transmembrane protein cargo of ILVs (Supplemental Figure S3; Odorizzi *et al.*, 1998). The functionality of the ILV budding pathway indicated by Cps1 sorting also confirmed that the VN and VC fusions did not disrupt the activities and Doa4 or Vps20, respectively, although it also possible that sufficient quantities of Doa4-VN not bound to Vps20-VC are present at steady state. Of note, the vacuolar lumen localization of Doa4-VN/Vps20-VC complexes was not an obligate outcome of split-Venus assemblies involving either Doa4-VN or Vps20-VC, nor was it unique to the Doa4-VN–Vps20-VC combination, because Doa4-VN coexpressed with Snf7-VC localized to puncta, whereas Doa4-VN coexpressed with Bro1-VC was localized within the vacuole lumen (Supplemental Figure S4).

To confirm that the Doa4-VN/Vps20-VC complexes required ILV sorting to be delivered into the vacuole lumen, we coexpressed the dominant-negative *vps4-E233Q* allele, which encodes a mutant version of Vps4 unable to hydrolyze ATP (Babst *et al.*, 1997). The consequence of *vps4-E233Q* expression is a block in ILV budding, which causes mislocalization of cargoes to aberrant endosomal puncta located adjacent to vacuoles. Figure 5A shows that *vps4-E233Q* expression caused a similar shift in BiFC fluorescence from vacuoles to endosomal puncta, where the BiFC fluorescence also colocalized with the ILV cargo, Cps1 (Supplemental Figure S3).

The results from BiFC studies shown in Figure 5A indicated that Doa4 and Vps20 must dissociate from one another to avoid their

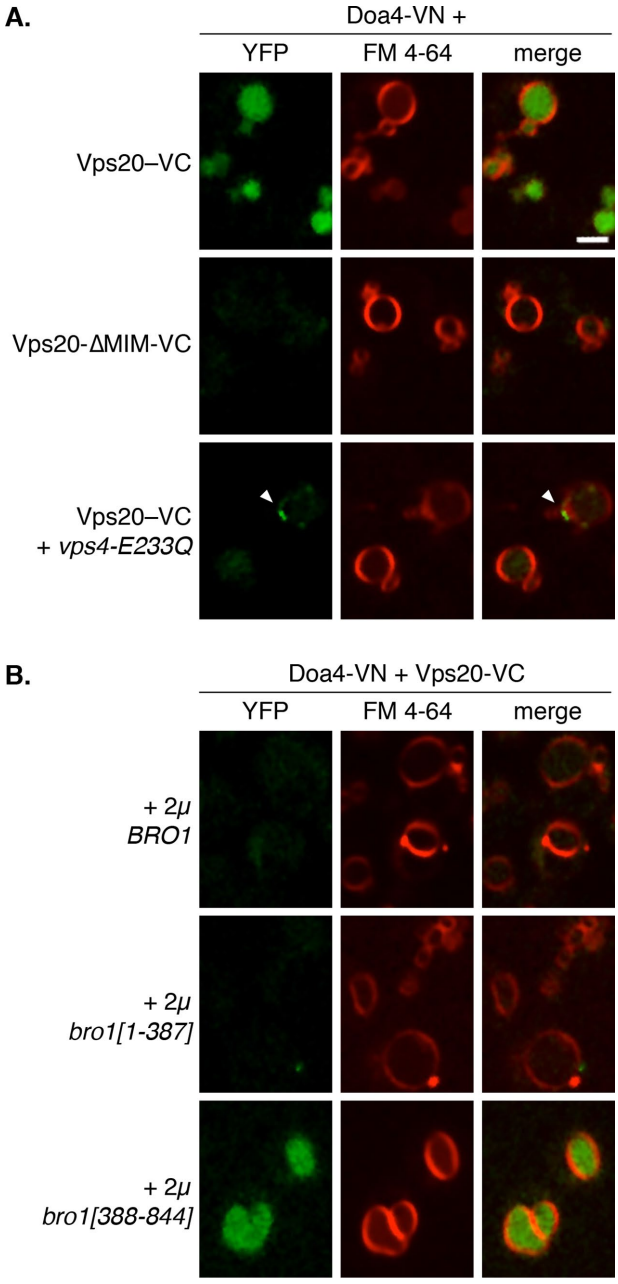

FIGURE 5: Bro1 relieves Vps20-inhibitory binding to Doa4. (A) Venus fluorescence derived from BiFC in yeast expressing Doa4-VN together with either wild-type Vps20-VC or mutant Vps20-ΔMIM1-VC. Endosome and vacuole membranes are stained with FM 4-64. Bottom row, cells transformed with a plasmid encoding the dominant-negative *vps4-E233Q* allele, which blocks the ILV budding pathway. The arrowhead indicates localization of BiFC fluorescence at endosomes stained with FM 4-64. (B) Venus fluorescence derived from BiFC between Doa4-VN and Vps20-VC in FM 4-64–stained wild-type yeast transformed with a high–copy number plasmid (*2μ*) encoding wild-type Bro1 vs. the amino-terminal Bro1 domain of Bro1 (*bro1[1-387]*) or the carboxyl-terminal V-Pro region of Bro1 (*bro1[388-844]*). Bar, 2 μm.

erroneous inclusion within ILVs. A mechanism must exist, therefore, that disrupts this interaction. We reasoned that the overproduction of a protein normally responsible for relieving Doa4 binding to Vps20 would block BiFC fluorescence between Doa4-VN and Vps20-VC, and a strong candidate for this role was Bro1, given that the inhibitory effect Vps20 has toward Doa4 is most evident in *bro1Δ* cells (Richter *et al.*, 2013; Figure 4). Supporting this hypothesis, we found that BiFC fluorescence in the vacuole lumen of cells expressing Doa4-VN and Vps20-VC was absent when the *BRO1* gene was overexpressed in this strain (Figure 5B).

We further queried which region of Bro1 blocks the Doa4-VN/Vps20-VC interaction by assaying BiFC fluorescence in cells overexpressing different functional domains of Bro1. The carboxyl-terminal proline-rich region of Bro1 binds directly to the Doa4 catalytic domain to stimulate its ubiquitin hydrolase activity (Richter *et al.*, 2007). However, overexpression of this region (Bro1[388-844]) had no apparent effect on BiFC fluorescence (Figure 5B). In contrast, BiFC fluorescence was abrogated upon overexpression of the amino-terminal Bro1 domain (Bro1[1-387]; Figure 5B), which is the region of Bro1 that binds the Snf7 subunit of ESCRT-III (Kim *et al.*, 2005). The ability of Bro1-domain overexpression to interfere with Vps20 binding by Doa4 might explain our previous finding that Bro1-domain overexpression caused a mild defect in ILV cargo sorting (Wemmer *et al.*, 2011). The timing with which Doa4 is released from its interaction with Vps20 may therefore be important for maintaining efficient function of the ILV-budding pathway.

Doa4 binds the open/active conformation of Vps20

Biochemical studies showed that the yeast Vps20 protein has a closed/inactive conformation that transitions to an open/active state in order to nucleate Snf7 polymerization (Saksena *et al.*, 2009; Teis *et al.*, 2010). Each of these conformational states for Vps20 can be stabilized by intragenic mutation (Figure 6A; Saksena *et al.*, 2009), which we exploited in order to test whether Doa4 preferentially binds Vps20 in its open/active versus closed/inactive conformation. A fusion protein consisting of glutathione *S*-transferase (GST) fused to Doa4 amino acids 2–80 (the region of Doa4 that binds the Vps20 MIM1 sequence; Richter *et al.*, 2013) was coexpressed in bacteria with wild-type Vps20, the constitutively closed/inactive Vps20-PW protein (containing the P183W, P189W, and P192W substitutions), or the constitutively open/active Vps20-Δloop protein (in which amino acids 48–59 had been deleted). Pull downs from bacterial lysates using glutathione–Sepharose showed that GST-Doa4[2-80] interacted with wild-type Vps20 and with the mutant Vps20-Δloop protein, whereas the mutant Vps20-PW protein failed to bind (Figure 6B). Thus Doa4 preferentially binds the open/active conformation of Vps20, which nucleates Snf7 polymerization.

The open/active conformation of Vps20 inhibits Doa4 function in the ILV budding pathway

To test whether Doa4 function in the ILV-budding pathway is affected by constitutive expression of Vps20 locked in either its open/active or closed/inactive conformation, we first examined the localization of GFP fused to the ILV cargo, Cps1. Figure 7A shows GFP-Cps1 localization to the vacuole lumen in wild-type yeast and in cells expressing the closed/inactive *vps20-PW* allele in place of wild-type *VPS20*. Electron tomography confirmed that *vps20-PW* cells have ILVs, albeit fewer than in wild-type cells (Figure 7, B and E). Thus the mutant Vps20-PW protein largely retains functionality under native conditions at endosomal membranes, even though purified Vps20-PW protein cannot nucleate Snf7 polymerization in vitro (Saksena *et al.*, 2009).

As shown previously (Teis *et al.*, 2010), cells expressing the open/active mutant *vps20-Δloop* allele were defective in ILV cargo sorting, resulting in the mislocalization of GFP-Cps1 to the vacuole membrane and to endosomal puncta adjacent to the vacuole (Figure 7A). Electron tomography showed that *vps20-Δloop* expression also caused

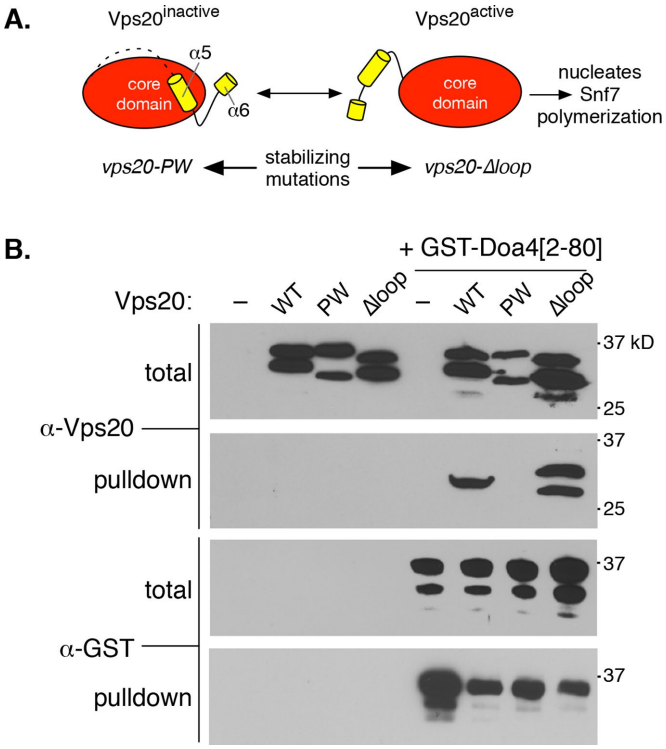

FIGURE 6: Doa4 binds the open/active conformation of Vps20. (A) Closed/inactive vs. open/active conformations of Vps20, each of which is stabilized by mutations (Vps20-PW and Vps20-Δloop, respectively). (B) Glutathione–Sepharose pull downs from lysates of bacteria expressing wild-type or mutant Vps20 protein; coexpression of GST-Doa4[2-80] is indicated at the top. Each of the Vps20 proteins exhibited spurious proteolysis when isolated from bacteria, resulting in lower–molecular weight fragments in addition to full-length proteins. For reasons that are unclear, GST-Doa4[2-80] binds only the fragmented form of wild-type Vps20, but binds both the full-length and fragmented form of Vps20-Δloop. Data are from a representative experiment performed in triplicate.

formation of class E compartments that contained very few ILVs (Figure 7, C and E). Class E compartments are diagnostic of ESCRT dysfunction in yeast and consist of aberrant stacks of flattened endosomal "cisternae" that correspond to the fluorescent puncta at which missorted Cps1 and other cargoes accumulate (Raymond *et al.*, 1992; Rieder *et al.*, 1996; Figure 7A). Of importance, mutation of the Doa4-binding MIM1 sequence in the loop-mutant form of Vps20 (*vps20-Δloop;ΔMIM1*) resulted in the recovery of GFP-Cps1 localization within the vacuole lumen (Figure 7A) and suppressed class E compartment formation, resulting in the rescue of normal endosomal morphology and improved ILV budding efficiency (Figure 7, D and E). These observations signify that the ILV cargo-sorting and budding defects caused by the open/active mutant Vps20-Δloop protein are due to its inhibitory binding to Doa4.

We also tested whether constitutive expression of the open/active *vps20-Δloop* allele affected the deubiquitination of ILV cargoes by Doa4. In principle, we expected *vps20-Δloop* would have no effect on deubiquitination because our data obtained thus far indicated that Vps20-binding inhibits the ability of Doa4 to function noncatalytically toward stabilizing ESCRT-III. However, we found that the Cps1 cargo protein accumulated in its ubiquitinated state in *vps20-Δloop* cells as strongly as it did in cells expressing the catalytically inactive *doa4-C571S* allele (Figure 7F). Mutation of the Doa4-binding MIM1 site (*vps20-Δloop;ΔMIM1*) restored Cps1 deubiquitination, confirming that the constitutively open/active form of Vps20 inhibits Doa4-mediated deubiquitination of cargoes in the ILV-budding pathway (Figure 7F). Conversely, Cps1 deubiquitination was unaffected in cells expressing the *vps20-PW* allele (Figure 7F). These results therefore indicate that deubiquitination of ILV cargoes is inhibited by Doa4 binding to the open/active conformation of Vps20 that initiates ESCRT-III complex assembly.

DISCUSSION

ESCRT-III is an ancient and versatile membrane scission machine that functions in a growing list of membrane-remodeling pathways (Hurley, 2015). Although the biophysical mechanism of membrane scission by ESCRT-III is unknown, in vitro and in vivo studies support a model in which scission is dictated by the cycle of ESCRT-III assembly and disassembly (Sachse *et al.*, 2004; Hanson *et al.*, 2008; Wollert *et al.*, 2009; Wemmer *et al.*, 2011; Adell *et al.*, 2014; Cashikar *et al.*, 2014; Shen *et al.*, 2014). Our data suggest a role for Doa4 in stabilizing ESCRT-III complexes to slow the rate of ILV membrane scission. Assigning this new regulatory role endows Doa4 with the ability to coordinate the timing of ILV budding with cargo deubiquitination, thereby guarding against premature enclosure of ubiquitinated cargoes within ILVs severed from the limiting endosomal membrane by ESCRT-III (Figure 8). The importance this coordination has in cellular physiology is suggested by studies of *doa4Δ* mutant yeast, which are sensitive to a variety of stresses as a consequence of free, nonconjugated ubiquitin being severely depleted (Swaminathan *et al.*, 1999). That this sensitivity stems from ubiquitin depletion via the ILV-budding pathway is indicated by the recovery of stress resistance in *doa4Δ* cells having extragenic mutations that disable ESCRT-III function (Amerik *et al.*, 2000).

The ability of Doa4 to stabilize ESCRT-III complexes is inhibited through its interaction with Vps20, which nucleates Snf7 polymerization to initiate ESCRT-III assembly (Saksena *et al.*, 2009). This finding seems paradoxical because it suggests that Vps20 simultaneously promotes and inhibits ESCRT-III complex stability. However, we found that Vps20-binding also inhibits ILV cargo deubiquitination by Doa4. Based on the proposal that spiral assemblies of ESCRT-III complexes encircle cargoes to prevent their diffusion away from the site of ILV budding as the cargoes undergo deubiquitination (Teis *et al.*, 2010), our results indicate that Vps20 binding might primarily serve to limit Doa4 activity at the onset of ESCRT-III complex assembly to prevent the premature deubiquitination of ILV cargoes (Figure 8).

How might Doa4 inhibition by Vps20 be relieved? BiFC analysis suggests that Doa4 binding to Vps20 is negatively regulated by Bro1. This finding extends our understanding of the functional relationship between Doa4 and Bro1 in the ILV-budding pathway. Through its carboxyl-terminal region, Bro1 directly binds the Doa4 catalytic domain to stimulate ubiquitin hydrolase activity (Richter *et al.*, 2007). We now show the amino-terminal Bro1 domain promotes (directly or indirectly) Doa4 release from Vps20.

Bro1 also functions to stabilize ESCRT-III complexes through its interaction with Snf7 (Wemmer *et al.*, 2011), and it does so independently of its role in negatively regulating Doa4 binding to Vps20 because overexpression of *BRO1* restored ESCRT-III complex stability in cells lacking Doa4. Bro1 inhibits ESCRT-III disassembly, and as a consequence, the amount of ESCRT-III complexes seen in wild-type cells is increased in response to *BRO1* overexpression (Wemmer *et al.*, 2011). *DOA4* overexpression phenocopied this increase in ESCRT-III complex abundance but also caused the accumulation of higher–molecular weight ESCRT-III complexes that were not seen upon *BRO1* overexpression. Doa4 and Bro1 thus seem to regulate

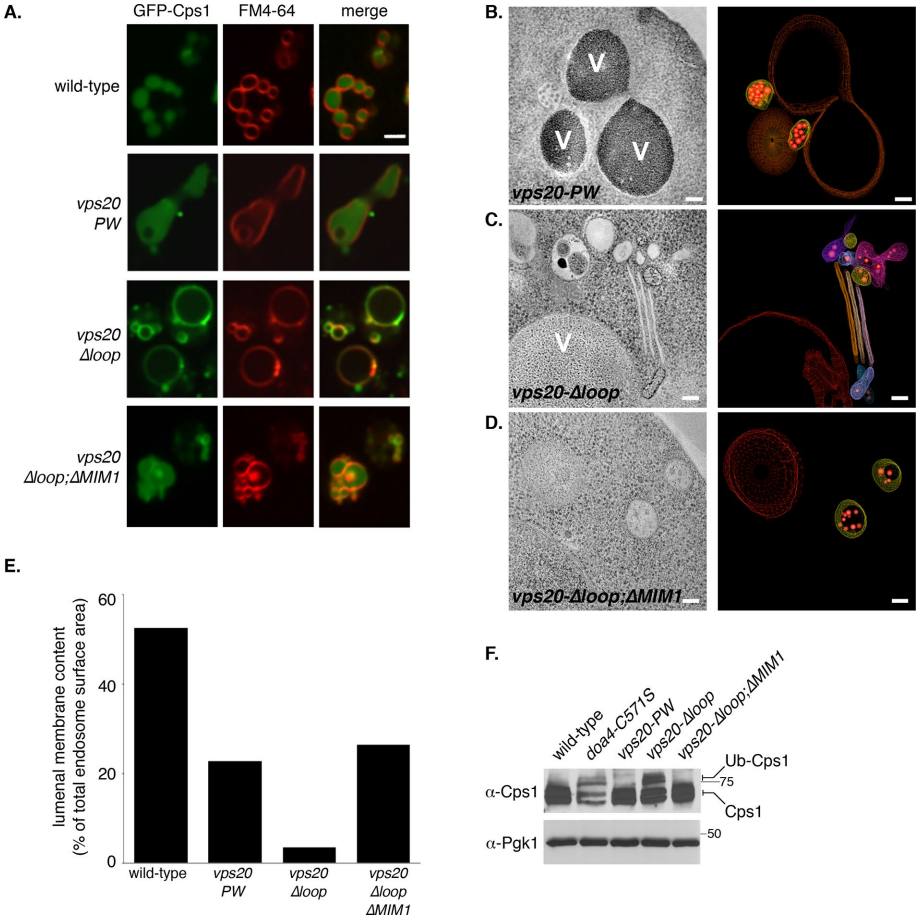

FIGURE 7: The open/active conformation of Vps20 inhibits Doa4 function in the ILV-budding pathway. (A) Fluorescence images of FM 4-64–stained yeast expressing GFP-Cps1. Bar, 2 μm. (B–D) Two-dimensional cross-sectional tomographic slices and 3D models as depicted in Figure 3; bar, 100 nm. (E) Quantitation of the lumenal percentage of total endosome membrane area. (F) Western blot analysis of Cps1 vs. 3-phosphoglycerate kinase (Pgk1) in total-cell lysates. The *PEP4* and *PRB1* genes were deleted in each strain to prevent spurious cleavage of ubiquitinated Cps1 (Ub-Cps1) upon vacuolar disruption during cell lysis. Cps1 in both its nonubiquitinated and ubiquitinated forms migrates as a doublet due to differential glycosylation (Spormann *et al.*, 1992).

ESCRT-III by different mechanisms, although neither mechanism has been determined. We found that neither *DOA4* nor *BRO1* overexpression rescued ESCRT-III complex stability in the absence of ESCRT-II–mediated activation of Vps20 (this study; Wemmer *et al.*, 2011), but purified Bro1 can promote Snf7 polymerization in vitro (Tang *et al.*, 2016). Therefore Bro1 might boost the levels of ESCRT-III complexes by stimulating assembly in addition to stabilizing ESCRT-III complexes directly through binding to Snf7 (Wemmer *et al.*, 2011) and indirectly by promoting the relief of inhibitory binding between Doa4 and Vps20 (this study). We have not investigated whether Doa4, like Bro1, affects Snf7 polymerization in vitro.

Given the central role of ESCRT-III in ILV budding, the function we describe for Doa4 in regulating ESCRT-III would seem at odds with our previous work showing that ILV budding does not require Doa4 (Richter *et al.*, 2007). However, the depletion of free, nonconjugated ubiquitin seen in the absence of Doa4 (Swaminathan *et al.*, 1999) constricts the influx of ubiquitinated transmembrane proteins into the ILV-budding pathway (Katzmann *et al.*, 2004). Because the production of ILVs depends on ubiquitinated ILV cargoes (MacDonald *et al.*, 2012), a reduction in cargo influx stemming from the loss of Doa4 might prove inconsequential to ESCRT-III function, especially given our results showing that Bro1 acts independently of Doa4 to regulate ESCRT-III. The absence of Doa4 would be expected to have greater effect in the face of higher demand for ESCRT-III function in the ILV-budding pathway. Indeed, increasing the influx of ubiquitinated cargoes by genetic repletion of free ubiquitin levels inhibits ILV budding in cells lacking Doa4 function (Richter *et al.*, 2007).

Our model positions Doa4 and Bro1 at both the beginning and the end of ESCRT-III function in the ILV-budding pathway of yeast (Figure 8), but several questions remain. For instance, what triggers Bro1 to relieve Doa4 from inhibitory binding by Vps20? Knowing this information would give insight into the state of ESCRT-III assembly at which Doa4 and Bro1 functionally cooperate. Conversely, what terminates Doa4/Bro1 regulation of ESCRT-III? Based on the delay in ILV membrane scission seen upon overexpression of either *DOA4* (this study) or *BRO1* (Wemmer *et al.*, 2011), their negative regulation seems necessary for timely completion of the ILV budding process. As mentioned earlier, how Doa4 and Bro1 regulate ESCRT-III complex stability is unknown. Like Bro1, Doa4 can bind Snf7 (Bowers *et al.*, 2004; Wolters and Amerik, 2015), and this interaction might serve as the basis for Doa4 interacting with ESCRT-III when both Bro1 and the Doa4-binding MIM1 sequence in Vps20 are absent (Richter *et al.*, 2013); however, the possibility that Doa4 and/or Bro1 restricts access of polymeric Snf7 to the Vps4 disassembly ATPase has been complicated by the low-affinity interaction between Vps4 and Snf7 (Kojima *et al.*, 2016; Schöneberg *et al.*, 2017).

Our results might offer insight into the mechanism by which certain plus-stranded RNA viruses replicate. Proteins encoded by the tomato bushy stunt virus (TBSV) and brome mosaic virus (BMV) recruit ESCRT-III in plants to the cytosolic surface of peroxisomes and the endoplasmic reticulum, respectively, where the viruses exploit ESCRT-III to create membrane invaginations that protect the viral replication machinery away from the cytosol (Barajas *et al.*, 2009; Diaz *et al.*, 2015). These budded replication compartments, however, are not severed. Our finding that Doa4 and Bro1 can inhibit membrane scission by regulating ESCRT-III stability raises the possibility that a similar mechanism might be used by TBSV and BMV to maintain their budded replication compartments as nonsevered invaginations. In support of this hypothesis, both TBSV and BMV can replicate in yeast, and this process requires Doa4 and Bro1 (Kushner *et al.*, 2003; Panavas *et al.*, 2005). For BMV, the activities Doa4 and Bro1 have in maintaining ubiquitin homeostasis were found to be important for viral replication (Wang *et al.*, 2011), but, as in the ILV-budding pathway, the functions Doa4 and Bro1 have in deubiquitination and ESCRT-III regulation need not be mutually exclusive.

Do orthologues of Doa4 and Bro1 also regulate ESCRT-III function in other organisms? The mammalian Bro1 orthologue, ALIX,

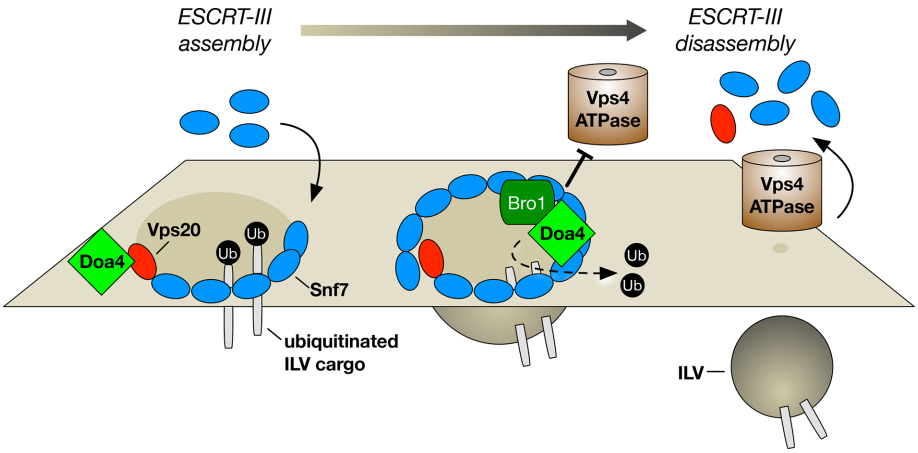

FIGURE 8: Proposed model for Doa4 regulation and function in the ILV-budding pathway. We propose that the open/active conformation of Vps20, which nucleates Snf7 polymerization, binds Doa4 to restrict Doa4 access to ubiquitinated ILV cargoes at the onset of ESCRT-III assembly. We also propose that Bro1 (directly or indirectly) relieves inhibitory binding to Doa4 by Vps20. Bro1 stimulates Doa4 ubiquitin hydrolase activity (Richter *et al.*, 2007), and we propose that during the period of cargo deubiquitination, Doa4 and Bro1 stabilize ESCRT-III by inhibiting disassembly of the complex by Vps4. ESCRT-III disassembly is linked to membrane scission, which completes the ILV-budding process. Note that the timing of Doa4 and Bro1 interactions portrayed in this model has yet to be established.

seems to operate in this capacity at the plasma membrane, where it recruits CHMP4B, a Snf7 orthologue that functions in ESCRT-III–mediated membrane scission during the abscission step of cytokinesis (Carlton *et al.*, 2012). ALIX also recruits the CHMP4C paralogue, which is a checkpoint component that interferes with CHMP4B function to delay abscission until chromatin is cleared from the intercellular bridge connecting daughter cells (Christ *et al.*, 2016). Like Bro1 in yeast, therefore, ALIX might regulate the timing of ESCRT-III plasma membrane scission activity, albeit through a different mechanism. Future studies may reveal whether ESCRT-III is also regulated at endosomes in mammalian cells by ALIX or UBPY, the apparent functional orthologue of Doa4.

MATERIALS AND METHODS

Yeast strains and plasmid construction

Standard techniques were used for the growth and genetic manipulation of *S. cerevisiae* strains (Table 1) and for the construction of plasmids (Table 2). Yeast strains created for this study were constructed by one-step PCR-based integration using cassettes described in Longtine *et al.* (1998) and Webster *et al.* (2014). The 2μ *bro1(388-844)* plasmid encoding the carboxyl-terminal V-Pro region of Bro1 was constructed using the gene splicing by overlap extension method of PCR (geneSOE; Higuchi *et al.*, 1988) to fuse 500 base pairs of the *BRO1* 5′ untranslated region plus the start codon in-frame with the coding sequence for Bro1 amino acids 388–844, and the full sequence was cloned into the *SpeI*/*SalI* site of pRS426 (Christianson *et al.*, 1992), resulting in the plasmid pGO642. To construct plasmids encoding the *vps20-PW* and *vps20-Δloop* alleles, the epitope-tagged versions of each allele described in Teis *et al.* (2010) were used as templates for PCR to generate copies that replaced the epitope tag with a stop codon, and the resulting full sequences of each nontagged allele were cloned into the *SacI* site of pRS414 (Christianson *et al.*, 1992), resulting in the plasmids pGO829 and pGO830. To construct bacterial expression plasmids, PCR products consisting of a Shine–Dalgarno sequence followed by the coding sequences for *VPS20*,

Strain	Genotype	Reference
SEY6210	*MATα leu2-3,112 ura3-52 his3Δ200 trp1-Δ901 lys2-Δ801 suc2-Δ9*	Robinson *et al.* (1988)
GOY65	SEY6210; *bro1Δ::HIS3*	Odorizzi *et al.* (2003)
GOY248	SEY6210; $vps20^{\Delta MIM1}$*::KANMX6*	Richter *et al.* (2013)
GOY250	SEY6210; $vps20^{\Delta MIM1}$*::KANMX6 bro1Δ::HIS3*	Richter *et al.* (2013)
GOY307	SEY6210; $vps20^{\Delta MIM1}$*::KANMX6 bro1Δ::TRP1 doa4Δ::KANMX6*	Richter *et al.* (2013)
DBY5	SEY6210; *doa4Δ::HIS3*	Richter *et al.* (2007)
DBY6	SEY6210; *doa4Δ::HIS3 vps4Δ::TRP1*	Richter *et al.* (2007)
MBY3	SEY6210; *vps4Δ::TRP1*	Babst *et al.* (1997)
EEY2-1	SEY6210; *vps20Δ::HIS3*	Babst *et al.* (2002b)
GOY445	SEY6210; *VPS20-VC::KANMX6 DOA4-VN::HIS3MX6*	This study
GOY454	SEY6210; $vps20^{\Delta MIM1}$*-VC::KANMX6 DOA4-VN::HIS3MX6*	This study
GOY471	SEY6210; $vps20^{PW}$*-VC::KANMX6 DOA4-VN::HIS3MX6*	This study
GOY472	SEY6210; $vps20^{loop}$*-VC::KANMX6 DOA4-VN::HIS3MX6*	This study
GOY477	SEY6210; $vps20^{loop;\Delta MIM1}$	This study
MMY14	SEY6210; *pep4Δ::LEU2 prb1Δ::LEU2 SNA3-GFP::KANMX6*	McNatt *et al.* (2007)
MMY60	SEY6210; *pep4Δ::LEU2 prb1Δ::LEU2 SNA3-GFP::KANMX6* $doa4^{C571S}$	McNatt *et al.* (2007)
GOY474	SEY6210; *pep4Δ::LEU2 prb1Δ::LEU2 SNA3-GFP::KANMX6 vps20Δ::HIS3MX6*	This study
GOY476	SEY6210; *pep4Δ::LEU2 prb1Δ::LEU2 SNA3-GFP::KANMX6* $vps20^{loop;\Delta MIM1}$*::HIS3MX6*	This study

TABLE 1: Yeast strains used in this study.

Plasmid	Description	Genotype	Reference
pRS416		*URA3* Ap^R *CEN*	Christianson *et al.* (1992)
pRS414		*TRP1* Ap^R *CEN*	Christianson *et al.* (1992)
pRS426		*URA3* Ap^R *2μ*	Christianson *et al.* (1992)
pST39		Ap^R	Tan (2001)
pCR64	*CEN doa4*$^{C/S}$	*URA3* Ap^R *(pRS416) doa4*^{C571S}	Richter *et al.* (2007)
pMB103	*2μ vps4*$^{E/Q}$	*URA3* Ap^R *(pRS426) vps4*^{E233Q}	Babst *et al.* (1997)
pGO216	*2μ BRO1*	*URA3* Ap^R *(pRS426) BRO1*	Wemmer *et al.* (2011)
pGO642	*2μ bro1*$^{388-844}$	*URA3* Ap^R *(pRS426) bro1*$^{388-844}$	This study
pMWM3	*2μ bro1*$^{1-387}$	*URA3* Ap^R *(pRS426) bro1*$^{1-387}$	Wemmer *et al.* (2011)
pGO511	Vps20	Ap^R (pST39) *VPS20*	This study
pGO816	Vps20^{PW}	Ap^R (pST39) *vps20*^{P183W,P189W,P192W}	This study
pGO817	Vps20^{loop}	Ap^R (pST39) *vps20*$^{\Delta 48-59}$	This study
pGO818	GST-Doa4$^{2-80}$	Ap^R (pST39) *GST-doa4*$^{2-80}$	This study
pGO819	Vps20; GST-Doa4$^{2-80}$	Ap^R (pST39) *VPS20 GST-doa4*$^{2-80}$	Babst *et al.* (1997)
pGO820	Vps20^{PW}; GST-Doa4$^{2-80}$	Ap^R (pST39) *ps20*^{P183W,P189W,P192W} *GST-doa4*$^{2-80}$	Babst *et al.* (2002b)
pGO826	Vps20^{loop}; GST-Doa4$^{2-80}$	Ap^R (pST39) *vps20*$^{\Delta 48-59}$ *GST-doa4*$^{2-80}$	This study
pGO45	*2μ GFP-CPS1*	*URA3* Ap^R (pRS426) *GFP-CPS1*	Odorizzi *et al.* (1998)
pGO829	*CEN vps20*^{PW}	*TRP1* Ap^R (pRS414) *vps20*^{P183W,P189W,P192W}	This study
pGO830	*CEN vps20*^{loop}	*TRP1* Ap^R (pRS414) *vps20*$^{\Delta 48-59}$	This study

TABLE 2: Plasmids used in this study.

vps20-PW, or *vps20-Δloop* were created from wild-type genomic DNA, pGO829, or pGO830 templates, respectively, and then cloned into the *Sac*I/*Kpn*I site of pST39 (Tan, 2001), resulting in the plasmids pGO511, pGO816, and pGO817. The coding sequence for GST-Doa4(2-80) from template pCR152 (Richter *et al.*, 2013) was cloned Into the *Bsp*EI/*Mlu*I site of pST39 or the Vps20-encoding pST39 plasmids, resulting in the plasmids pGO818, pGO819, pGO820, and pGO826.

Rate-zonal density gradient analysis of ESCRT-III

Thirty OD_{600} units of yeast cells were converted to spheroplasts, osmotically lysed in 1 ml of ice-cold lysis buffer consisting of phosphate-buffered saline (PBS; 137 mM NaCl, 2.7 mM KCl, 10 mM Na_2HPO_4, 1.8 mM KH_2PO_4), pH 7.4, that was supplemented with 0.5% Tween-20 and a protease inhibitor cocktail (Roche Diagnostics, Switzerland). The cells were then homogenized on ice before centrifugation at 16,100 × *g* for 10 min at 4°C to pellet membranes. The membrane fraction was resuspended in 1 ml of ice-cold lysis buffer and passed five times through a 25-gauge needle to generate a solubilized protein sample that was loaded at the top of a linear glycerol gradient (10–40%) prepared in PBS and 0.5% Tween-20. The gradient was centrifuged at 100,000 × *g* for 4 h at 4°C, and then 1-ml fractions were collected from the top of the gradient, and 10% (vol/vol) trichloroacetic acid (TCA) was added to precipitate the proteins on ice for 20 min. The precipitates were harvested by centrifugation at 16,100 × *g* for 10 min at 4°C and then resuspended by sonication into ice-cold acetone and incubated on ice for 20 min. Precipitates were harvested by centrifugation and sonication into acetone once more, after which the pellets were dried by rotary evaporation; then, each was resuspended by sonication into 100 μl of Laemmli buffer (0.1% β-mercaptoethanol, 0.0005% bromophenol blue, 10% glycerol, 2% SDS, 63 mM Tris-HCl, pH 6.8). The gradient fraction protein samples were boiled for 5 min, and 10 μl of each was resolved by SDS–PAGE, transferred to nitrocellulose, and analyzed by Western blot using anti-Snf7 polyclonal antiserum (Babst *et al.*, 1998). Detection of Snf7 in each fraction was performed by incubating nitrocellulose with Alexa Fluor 680 secondary antibody (Invitrogen) and then visualizing with an infrared imager (Odyssey; LI-COR Biosciences). The amount of Snf7 was quantitated in triplicate experiments with Odyssey software (version 2.1). Calibration of the gradient was performed using aldolase (158 kDa), catalase (232 kDa), and ferritin (440 kDa) (GE Healthcare; United Kingdom).

Electron microscopy and tomography

Liquid cultures of yeast cells were harvested at logarithmic phase, vacuum-filtered on 0.45-μm Millipore paper, loaded into 0.25-mm aluminum planchettes, and high-pressure frozen in a Balzers Bal-Tec HPM 010 (Boeckeler Instruments, Tucson, AZ). A Leica AFS system (Leica, Austria) was used for freeze-substitution preparation of 0.1% uranyl acetate and 0.25% glutaraldehyde in anhydrous acetone (Giddings, 2003). Samples were then washed in pure acetone, embedded in Lowicryl HM20 resin (Polysciences, Warrington, PA), and polymerized at 260°C. A Leica Ultra-Microtome was used to cut 250-nm serial semithick sections, which were collected onto 1% Formvar films and adhered to rhodium-plated copper grids (Electron Microscopy Sciences, Hatfield, PA). Grids were labeled on both sides with fiduciary 15-nm colloidal gold (British Biocell International, United Kingdom). Typically, *Z*-shrinkage of semithick sections was 20% volume and corrected in final models and measurements. Dual-axis tilt series were collected from 660° with 1° increments at 200 kV using a Tecnai F20 (FEI, Netherlands) at a magnification of 29,000x using SerialEM (Mastronarde, 2005). The use of 2× binning on the recording 4K × 4K charge-coupled device (CCD) camera (Gatan, United Kingdom) creates a 2000 × 2000 image with a pixel size of 0.764 nm. Dual-axis electron tomograms (Mastronarde, 1997) of endosomes and ILVs required the IMOD package (Kremer *et al.*, 1996)

for tomogram construction and modeling (3DMOD 4.0.11). Manually assigned contours of the endosomal limiting membrane at the inner leaflet were used to measure the surface of the bilayers periodically every 3.85 nm and calculated using imodmesh. Best-fit sphere models were used to measure the diameters of nearly spherical lumenal vesicles from the outer leaflet of the membrane bilayers (O'Toole *et al.*, 2002). IMODINFO provided surface area and volume data of contour models. Data were sorted, analyzed, and graphed using Excel (Microsoft, Redmond, WA) and Prism 5 (GraphPad Software, La Jolla, CA).

Fluorescence microscopy

Liquid cultures of yeast strains were grown to logarithmic phase at 30°C before observation at room temperature using a Nikon TE2000-U inverted fluorescence microscope equipped with a Yokogawa CSU-Xm2 spinning-disk confocal unit and a 100× oil objective with a numerical aperture of 1.4 (Nikon Instruments, Melville, NY). Fluorescence images were acquired with a Photometrics (Tucson, AZ) Cascade II electron-multiplying CCD camera using MetaMorph (version 7.0) software (Molecular Devices, Sunnyvale, CA) and then processed with ImageJ (National Institutes of Health, Bethesda, MD) and Photoshop CS4 software (Adobe Systems, Mountain View, CA). Endosomal membranes were stained with FM 4-64 (Invitrogen, Carlsbad, CA) using a 20-min pulse and 90-min chase (Odorizzi *et al.*, 2003).

Affinity purification of recombinant proteins expressed in bacteria

Vps20, Vps20-PW, and Vps20-Δloop proteins were expressed without or with GST-Doa4(2-80) in 5-ml liquid cultures of *Escherichia coli* BL21-CodonPlus (DE3) cells (Agilent Technologies, Santa Clara, CA) by induction with 0.5 mM isopropyl β-D-1-thiogalactopyranoside at 20°C for 18 h. Bacterial cells were harvested by centrifugation at 1800 × *g* for 10 min at 4°C and then lysed by resuspension on ice in 1 ml PBS supplemented with 1 mg/ml lysozyme (Roche Diagnostics), 0.25 U of Benzonase nuclease (Sigma-Aldrich, St. Louis, MO), and 1 mM phenylmethanesulfonyl fluoride (Sigma-Aldrich). Lysates were subjected to probe sonication at 15 W for 20 s. Then, 0.2% Triton X-100 (TX-100) was added, and the lysates were rotated at 4°C for 10 min before being clarified by centrifugation at 16,100 × *g* for 10 min at 4°C. The resulting supernatants were mixed with glutathione–Sepharose beads (GE Healthcare) and rotated at 4°C for 1 h. The beads were then washed thrice by centrifugation at 5000 × *g* for 1 min, resuspended in 1 ml of ice-cold PBS containing 0.2% TX-100, and then washed twice in 1 ml of ice-cold PBS. Washed beads were dried by rotary evaporation, bound proteins were eluted by boiling for 5 min in 100 µl Laemmli buffer, and 10 µl of each sample was resolved by SDS–PAGE, transferred to nitrocellulose, and analyzed by Western blot using mouse anti-GST monoclonal antibodies (Invitrogen) or using custom rabbit anti-Vps20 polyclonal antiserum (Invitrogen) that was raised against the yeast Vps20 peptide sequences E_{19}VKRSKDEIHKF$_{30}$ and L_{113}KKLNKEFSNVDE$_{125}$.

Detection of ubiquitinated Cps1 in yeast cell lysates

Yeast cells lacking vacuolar hydrolase activity (*pep4Δ prb1Δ*) were grown logarithmically in liquid culture at 27°C, and then 10 OD_{600} units were harvested by centrifugation at 1800 × *g* for 5 min at room temperature, resuspended in 5 mM *N*-ethylmaleimide (Sigma-Aldrich), and precipitated by the addition of 10% (vol/vol) TCA followed by incubation on ice for 20 min. Cellular material was reprecipitated twice in acetone as described, dried by rotary evaporation, and then resuspended by sonication in 100 µl of Laemmli buffer. The cell walls in precipitates were disrupted by adding acid-washed glass beads (150–212 µm; Sigma-Aldrich) and mixing vigorously by vortex at room temperature for 15 min and then boiling for 5 min. Ten microliters of the protein sample was resolved by SDS–PAGE and analyzed by Western blotting with rabbit polyclonal anti-Cps1 antiserum (Cowles *et al.*, 1997) and mouse anti-Pgk1 monoclonal antibodies (Invitrogen).

ACKNOWLEDGMENTS

We thank Scott Emr and Patrick Lusk for plasmids. This work was funded by National Institutes of Health Grant R01GM-111335 to G.O.

REFERENCES

Adell MA, Vogel GF, Pakdel M, Müller M, Lindner H, Hess MW, Teis D (2014). Coordinated binding of Vps4 to ESCRT-III drives membrane neck constriction during MVB vesicle formation. J Cell Biol 205, 33–49.

Alam SL, Sun J, Payne M, Welch BD, Blake BK, Davis DR, Meyer HH, Emr SD, Sundquist WI (2004). Ubiquitin interactions of NZF zinc fingers. EMBO J 23, 1411–1421.

Amerik AY, Nowak J, Swaminathan S, Hochstrasser M (2000). The Doa4 deubiquitinating enzyme is functionally linked to the vacuolar protein-sorting and endocytic pathways. Mol Biol Cell 11, 3365–3380.

Babst M, Katzmann DJ, Estepa-Sabal EJ, Meerloo T, Emr SD (2002b). ESCRT-III: an endosome-associated heterooligomeric protein complex required for MVB sorting. Dev Cell 3, 271–282.

Babst M, Katzmann DJ, Snyder WB, Wendland B, Emr SD (2002a). Endosome-associated complex, ESCRT-II, recruits transport machinery for protein sorting at the multivesicular body. Dev Cell 3, 283–289.

Babst M, Sato TK, Banta LM, Emr SD (1997). Endosomal transport function in yeast requires a novel AAA-type ATPase, Vps4p. EMBO J 16, 1820–1831.

Babst M, Wendland B, Estepa EJ, Emr SD (1998). The Vps4p AAA ATPase regulates membrane association of a Vps protein complex required for normal endosome function. EMBO J 17, 2982–2993.

Barajas D, Jiang Y, Nagy PD (2009). A unique role for the host ESCRT proteins in replication of Tomato bushy stunt virus. PLoS Pathog 5, e1000705.

Bilodeau PS, Urbanowski JL, Winistorfer SC, Piper RC (2002). The Vps27p Hse1p complex binds ubiquitin and mediates endosomal protein sorting. Nat Cell Biol 4, 534–539.

Bowers K, Lottridge J, Helliwell SB, Goldthwaite LM, Luzio JP, Stevens TH (2004). Protein-protein interactions of ESCRT complexes in the yeast *Saccharomyces cerevisiae*. Traffic 5, 194–210.

Carlton JG, Caballe A, Agromayor M, Kloc M, Martin-Serrano J (2012). ESCRT-III governs the Aurora B-mediated abscission checkpoint through CHMP4C. Science 336, 220–225.

Carlton JG, Martin-Serrano J (2007). Parallels between cytokinesis and retroviral budding: a role for the ESCRT machinery. Science 316, 1908–1912.

Cashikar AG, Shim S, Roth R, Maldazys MR, Heuser JE, Hanson PI (2014). Structure of cellular ESCRT-III spirals and their relationship to HIV budding. Elife 3, e02184.

Chiaruttini N, Redondo-Morata L, Colom A, Humbert F, Lenz M, Scheuring S, Roux A (2015). Relaxation of loaded ESCRT-III spiral springs drives membrane deformation. Cell 163, 866–879.

Christ L, Wenzel EM, Liestøl K, Raiborg C, Campsteijn C, Stenmark H (2016). ALIX and ESCRT-I/II function as parallel ESCRT-III recruiters in cytokinetic abscission. J Cell Biol 212, 499–513.

Christianson TW, Sikorski RS, Dante M, Shero JH, Hieter P (1992). Multifunctional yeast high-copy-number shuttle vectors. Gene 110, 119–122.

Cowles CR, Snyder WB, Burd CG, Emr SD (1997). Novel Golgi to vacuole delivery pathway in yeast: identification of a sorting determinant and required transport component. EMBO J 16, 2769–2782.

Curtiss M, Jones C, Babst M (2007). Efficient cargo sorting by ESCRT-I and the subsequent release of ESCRT-I from multivesicular bodies requires the subunit Mvb12. Mol Biol Cell 18, 636–645.

Diaz A, Zhang J, Ollwerther A, Wang X, Ahlquist P (2015). Host ESCRT proteins are required for bromovirus RNA replication compartment assembly and function. PLoS Pathog 11, e1004742.

Dupre S, Haguenauer-Tsapis R (2001). Deubiquitination step in the endocytic pathway of yeast plasma membrane proteins: crucial role of Doa4p ubiquitin isopeptidase. Mol Cell Biol 21, 4482–4494.

Garrus JE, von Schwedler UK, Pornillos OW, Morham SG, Zavitz KH, Wang HE, Wettstein DA, Stray KM, Côté M, Rich RL, *et al.* (2001). Tsg101 and

the vacuolar protein sorting pathway are essential for HIV-1 budding. Cell 107, 55–65.
Giddings TH (2003). Freeze-substitution protocols for improved visualization of membranes in high-pressure frozen samples. J Microsc 212, 53–61.
Hanson PI, Cashikar A (2012). Multivesicular body morphogenesis. Annu Rev Cell Dev Biol 28, 337–362.
Hanson PI, Roth R, Lin Y, Heuser JE (2008). Plasma membrane deformation by circular arrays of ESCRT-III protein filaments. J Cell Biol 180, 389–402.
Henne WM, Buchkovich NJ, Zhao Y, Emr SD (2012). The endosomal sorting complex ESCRT-II mediates the assembly and architecture of ESCRT-III helices. Cell 151, 356–371.
Higuchi R, Krummel B, Saiki RK (1988). A general method of in vitro preparation and specific mutagenesis of DNA fragments: study of protein and DNA interactions. Nucleic Acids Res 16, 7351–7367.
Hurley JH (2015). ESCRTs are everywhere. EMBO J 34, 2398–2407.
Im YJ, Wollert T, Boura E, Hurley JH (2009). Structure and function of the ESCRT-II-III interface in multivesicular body biogenesis. Dev Cell 17, 234–243.
Jimenez AJ, Maiuri P, Lafaurie-Janvore J, Divoux S, Piel M, Perez F (2014). ESCRT machinery is required for plasma membrane repair. Science 343, 1247136.
Katzmann DJ, Babst M, Emr SD (2001). Ubiquitin-dependent sorting into the multivesicular body pathway requires the function of a conserved endosomal protein sorting complex, ESCRT-I. Cell 106, 145–155.
Katzmann DJ, Sarkar S, Chu T, Audhya A, Emr SD (2004). Multivesicular body sorting: ubiquitin ligase Rsp5 is required for the modification and sorting of carboxypeptidase S. Mol Biol Cell 15, 468–480.
Kerppola TK (2006). Design and implementation of bimolecular fluorescence complementation (BiFC) assays for the visualization of protein interactions in living cells. Nat Protoc 1, 1278–1286.
Kieffer C, Skalicky J, Morita E, Domenico I, Ward D, Kaplan J, Sundquist W (2008). Two distinct modes of ESCRT-III recognition are required for VPS4 functions in lysosomal protein targeting and HIV-1 budding. Dev Cell 15, 62–73.
Kim J, Sitaraman S, Hierro A, Beach BM, Odorizzi G, Hurley JH (2005). Structural basis for endosomal targeting by the Bro1 domain. Dev Cell 8, 937–947.
Kojima R, Obita T, Onoue K, Mizuguchi M (2016). Structural fine-tuning of MIT-interacting motif 2 (MIM2) and allosteric regulation of ESCRT-III by Vps4 in yeast. J Mol Biol 428, 2392–2404.
Kremer JR, Mastronarde DN, McIntosh JR (1996). Computer visualization of three-dimensional image data using IMOD. J Struct Biol 116, 71–76.
Kushner DB, Lindenbach BD, Grdzelishvili VZ, Noueiry AO, Paul SM, Ahlquist P (2003). Systematic, genome-wide identification of host genes affecting replication of a positive-strand RNA virus. Proc Natl Acad Sci USA 100, 15764–15769.
Longtine MS, McKenzie A, Demarini DJ, Shah NG, Wach A, Brachat A, Philippsen P, Pringle JR (1998). Additional modules for versatile and economical PCR-based gene deletion and modification in *Saccharomyces cerevisiae*. Yeast 14, 953–961.
Losko S, Kopp F, Kranz A, Kölling R (2001). Uptake of the ATP-binding cassette (ABC) transporter Ste6 into the yeast vacuole is blocked in the doa4 mutant. Mol Biol Cell 12, 1047–1059.
Luhtala N, Odorizzi G (2004). Bro1 coordinates deubiquitination in the multivesicular body pathway by recruiting Doa4 to endosomes. J Cell Biol 166, 717–729.
MacDonald C, Buchkovich NJ, Stringer DK, Emr SD, Piper RC (2012). Cargo ubiquitination is essential for multivesicular body intralumenal vesicle formation. EMBO Rep 13, 331–338.
Mastronarde DN (1997). Dual-axis tomography: an approach with alignment methods that preserve resolution. J Struct Biol 120, 343–352.
Mastronarde DN (2005). Automated electron microscope tomography using robust prediction of specimen movements. J Struct Biol 152, 36–51.
McNatt M, McKittrick I, West M, Odorizzi G (2007). Direct binding to Rsp5 mediates ubiquitin-independent sorting of Sna3 via the multivesicular body pathway. Mol Biol Cell 18, 697–706.
Obita T, Saksena S, Ghazi-Tabatabai S, Gill DJ, Perisic O, Emr SD, Williams RL (2007). Structural basis for selective recognition of ESCRT-III by the AAA ATPase Vps4. Nature 449, 735–739.
Odorizzi G, Babst M, Emr SD (1998). Fab1p PtdIns(3)P 5-kinase function essential for protein sorting in the multivesicular body. Cell 95, 847–858.
Odorizzi G, Katzmann DJ, Babst M, Audhya A, Emr SD (2003). Bro1 is an endosome-associated protein that functions in the MVB pathway in *Saccharomyces cerevisiae*. J Cell Sci 116, 1893–1903.
Olmos Y, Hodgson L, Mantell J, Verkade P, Carlton JG (2015). ESCRT-III controls nuclear envelope reformation. Nature 522, 236–239.
O'Toole ET, Winey M, McIntosh JR, Mastronarde DN (2002). Electron tomography of yeast cells. Methods Enzymol 351, 81–95.
Panavas T, Serviene E, Brasher J, Nagy P (2005). Yeast genome-wide screen reveals dissimilar sets of host genes affecting replication of RNA viruses. Proc Natl Acad Sci USA 102, 7326–7331.
Raymond CK, Howald-Stevenson I, Vater CA, Stevens TH (1992). Morphological classification of the yeast vacuolar protein sorting mutants: evidence for a prevacuolar compartment in class E *vps* mutants. Mol Biol Cell 3, 1389–1402.
Richter C, West M, Odorizzi G (2007). Dual mechanisms specify Doa4-mediated deubiquitination at multivesicular bodies. EMBO J 26, 2454–2464.
Richter C, West M, Odorizzi G (2013). Doa4 function in ILV budding is restricted through its interaction with the Vps20 subunit of ESCRT-III. J Cell Sci 126, 1881–1890.
Rieder SE, Banta LM, Köhrer K, McCaffery JM, Emr SD (1996). Multilamellar endosome-like compartment accumulates in the yeast *vps28* vacuolar protein sorting mutant. Mol Biol Cell 7, 985–999.
Robinson JS, Klionsky DJ, Banta LM, Emr SD (1988). Protein sorting in *Saccharomyces cerevisiae*: isolation of mutants defective in the delivery and processing of multiple vacuolar hydrolases. Mol Cell Biol 8, 4936–4948.
Sachse M, Strous GJ, Klumperman J (2004). ATPase-deficient hVPS4 impairs formation of internal endosomal vesicles and stabilizes bilayered clathrin coats on endosomal vacuoles. J Cell Sci 117, 1699–1708.
Saksena S, Wahlman J, Teis D, Johnson A, Emr S (2009). Functional reconstitution of ESCRT-III assembly and disassembly. Cell 136, 97–109.
Samson RY, Obita T, Freund SM, Williams RL, Bell SD (2008). A role for the ESCRT system in cell division in *Archaea*. Science 322, 1710–1713.
Schöneberg J, Lee I-HH, Iwasa JH, Hurley JH (2017). Reverse-topology membrane scission by the ESCRT proteins. Nat Rev Mol Cell Biol 18, 5–17.
Shen Q-TT, Schuh AL, Zheng Y, Quinney K, Wang L, Hanna M, Mitchell JC, Otegui MS, Ahlquist P, Cui Q, *et al.* (2014). Structural analysis and modeling reveals new mechanisms governing ESCRT-III spiral filament assembly. J Cell Biol 206, 763–777.
Shim S, Kimpler LA, Hanson PI (2007). Structure/function analysis of four core ESCRT-III proteins reveals common regulatory role for extreme C-terminal domain. Traffic 8, 1068–1079.
Spormann DO, Heim J, Wolf DH (1992). Biogenesis of the yeast vacuole (lysosome). The precursor forms of the soluble hydrolase carboxypeptidase yscS are associated with the vacuolar membrane. J Biol Chem 267, 8021–8029.
Stuchell-Brereton MD, Skalicky JJ, Kieffer C, Karren MA, Ghaffarian S, Sundquist WI (2007). ESCRT-III recognition by VPS4 ATPases. Nature 449, 740–744.
Swaminathan S, Amerik AY, Hochstrasser M (1999). The Doa4 deubiquitinating enzyme is required for ubiquitin homeostasis in yeast. Mol Biol Cell 10, 2583–2594.
Tan S (2001). A modular polycistronic expression system for overexpressing protein complexes in *Escherichia coli*. Protein Expr Purif 21, 224–234.
Tang S, Buchkovich NJ, Henne WM, Banjade S, Kim YJ, Emr SD (2016). ESCRT-III activation by parallel action of ESCRT-I/II and ESCRT-0/Bro1 during MVB biogenesis. Elife 5, e15507.
Teis D, Saksena S, Emr S (2008). Ordered assembly of the ESCRT-III complex on endosomes is required to sequester cargo during MVB formation. Dev Cell 15, 578–589.
Teis D, Saksena S, Judson BL, Emr SD (2010). ESCRT-II coordinates the assembly of ESCRT-III filaments for cargo sorting and multivesicular body vesicle formation. EMBO J 29, 871–883.
Vietri M, Schink KO, Campsteijn C, Wegner CS, Schultz SW, Christ L, Thoresen SB, Brech A, Raiborg C, Stenmark H (2015). Spastin and ESCRT-III coordinate mitotic spindle disassembly and nuclear envelope sealing. Nature 522, 231–235.
Wang X, Diaz A, Hao L, Gancarz B, den Boon JA, Ahlquist P (2011). Intersection of the multivesicular body pathway and lipid homeostasis in RNA replication by a positive-strand RNA virus. J Virol 85, 5494–5503.
Webster BM, Colombi P, Jäger J, Lusk CP (2014). Surveillance of nuclear pore complex assembly by ESCRT-III/Vps4. Cell 159, 388–401.
Wemmer M, Azmi I, West M, Davies B, Katzmann D, Odorizzi G (2011). Bro1 binding to Snf7 regulates ESCRT-III membrane scission activity in yeast. J Cell Biol 192, 295–306.
Wollert T, Hurley JH (2010). Molecular mechanism of multivesicular body biogenesis by ESCRT complexes. Nature 464, 864–869.
Wollert T, Wunder C, Lippincott-Schwartz J, Hurley JH (2009). Membrane scission by the ESCRT-III complex. Nature 458, 172–177.
Wolters N, Amerik A (2015). The N-terminal domains determine cellular localization and functions of the Doa4 and Ubp5 deubiquitinating enzymes. Biochem Biophys Res Commun 467, 570–576.